Supplement of Atmos. Chem. Phys., 24, 4231–4252, 2024
https://doi.org/10.5194/acp-24-4231-2024-supplement

Atmospheric Chemistry and Physics
Open Access
EGU

Supplement of

Atmospheric oxygen as a tracer for fossil fuel carbon dioxide: a sensitivity study in the UK

Hannah Chawner et al.

Correspondence to: Eric Saboya (eric.saboya@bristol.ac.uk) and Matthew Rigby (matt.rigby@bristol.ac.uk)

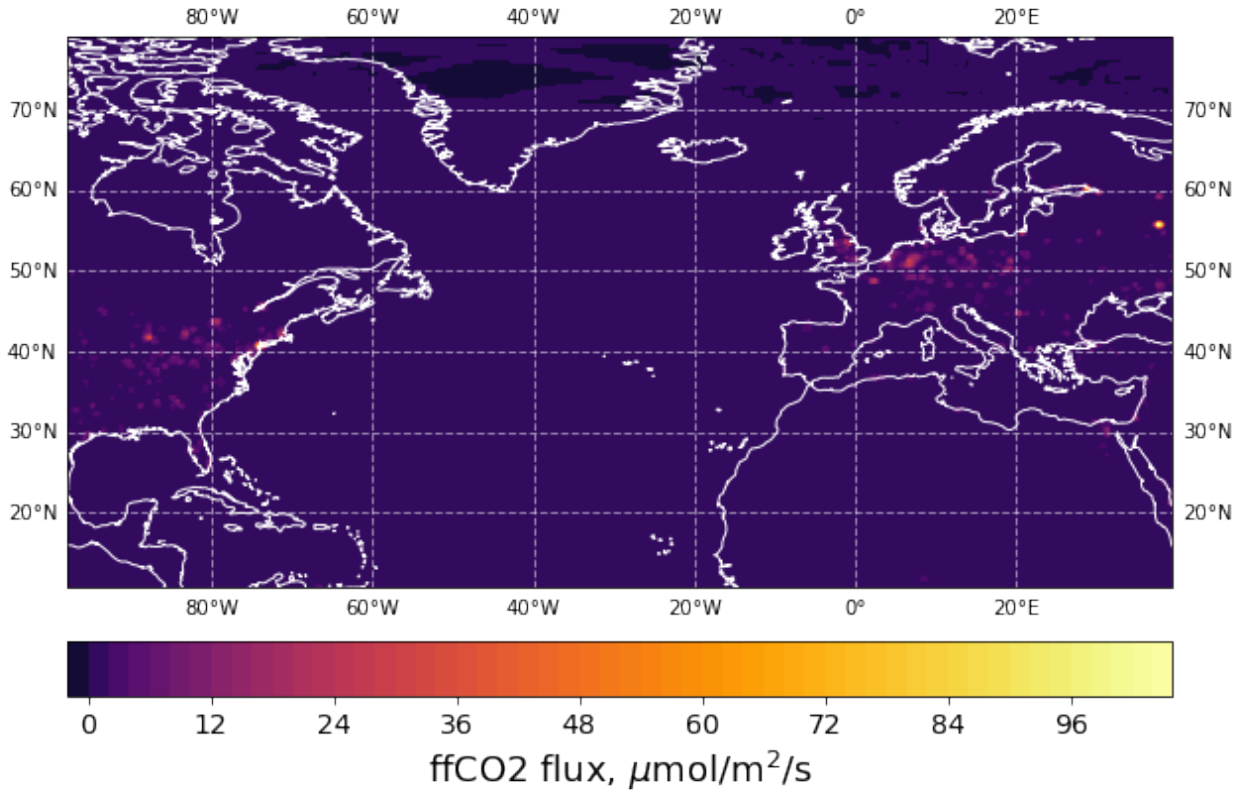

Figure 1. The fossil fuel CO_2 flux at one time step across the domain employed in this study.

1 The Model Domain

As discussed in Section 2.2.1 the NAME model that we use covers a longitude/latitude range: 10.729°- 79.057°N and 97.9°W - 39.38°E. An example of an emissions field across this domain is shown in Figure 1.

2 APO Timeseries

Here we model APO for the whole of 2015 at the three sites: Weybourne, Heathfield, and Ridge Hill. Firstly, a visualisation of the impact of our baseline "adjustment" is presented for Weybourne in Figure 2. Then, the simulations for all three sites are shown in Figure 3 for the APO models using the 3 ocean O_2 flux estimates: ECCO – Darwin (ED), Jena Carboscope (JC), and NEMO – ERSEM (NE), as well as including no contribution from the ocean. We also show the modelled and observed APO throughout 2015 as a scatter plot in Figure 4.

In Figure 5 we show the correlations between the modelled and observed CO_2 and O_2.

We also model APO throughout 2021, so as to compare the model with observational data from Heathfield, as shown in Figure 6. We note that we do not have ocean flux estimates for 2021 and here we instead rely on climatology data, averaged over the 2005-2015 period.

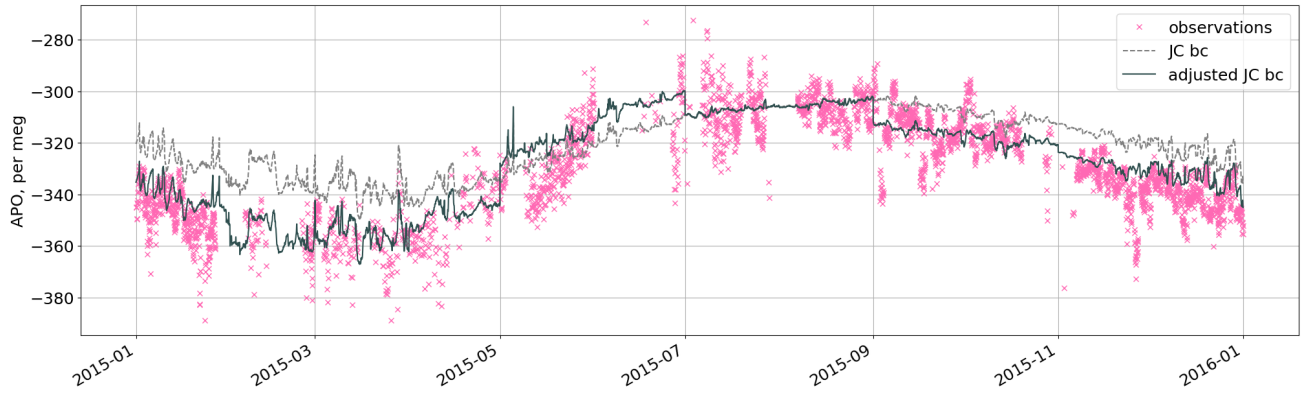

Figure 2. The APO observations (pink crosses) and baselines for 2015 at Weybourne. We show the baseline estimated by transporting boundary conditions from the Jena CarboScope APO inversion (JC, grey dotted line), and the adjusted version of this baseline (grey solid line).

3 Sensitivities

We have investigated the effects on our APO model of using three different estimates of the ocean O_2 flux. In Figure 7 we show the correlations between the models. As discussed in Section 3.4, we find that the largest difference and lowest correlation between the models is seen during the summer.

The ED and NE models both have daily and monthly outputs, providing the opportunity to investigate the impact of the flux resolution on our model. ED and NE fluxes are only available until 2018 and 2015, respectively, so for later years, our model will rely on climatologies (daily mean fields based on the period 2005 - 2015). We therefore also look at the difference in the oceanic contribution to the mole fraction when using climatologies compared to time-resolved fluxes.

Figure 8 shows the modelled ocean O_2 timeseries, comparing that using fluxes for the year of 2014 with those from a climatology, as well as those with a daily and monthly resolution from the ED and NE models. The top panel shows that at this time the contribution estimated by NE is significantly larger than that of ED for all variations of the models. However, during August, the contributions estimated by NE and ED more closely agree than JC, which estimates large periods of uptake.

Comparing the modelled timeseries using the climatology and the year-specific fluxes, we find that when using monthly fluxes there are differences in the O_2 uptake over the winter, whereas in the summer it makes very a small impact. However, the difference in the summer is larger when using higher resolution fluxes. This is true in particular for the NE model, for which the climatology underestimates more abrupt changes in the mole fraction contribution. The variability of the model using the daily climatology is more similar to that using monthly fluxes as oceanic outgassing events are smoothed out when averaging across multiple years, whereas more frequent, seasonal variations are captured by the climatology.

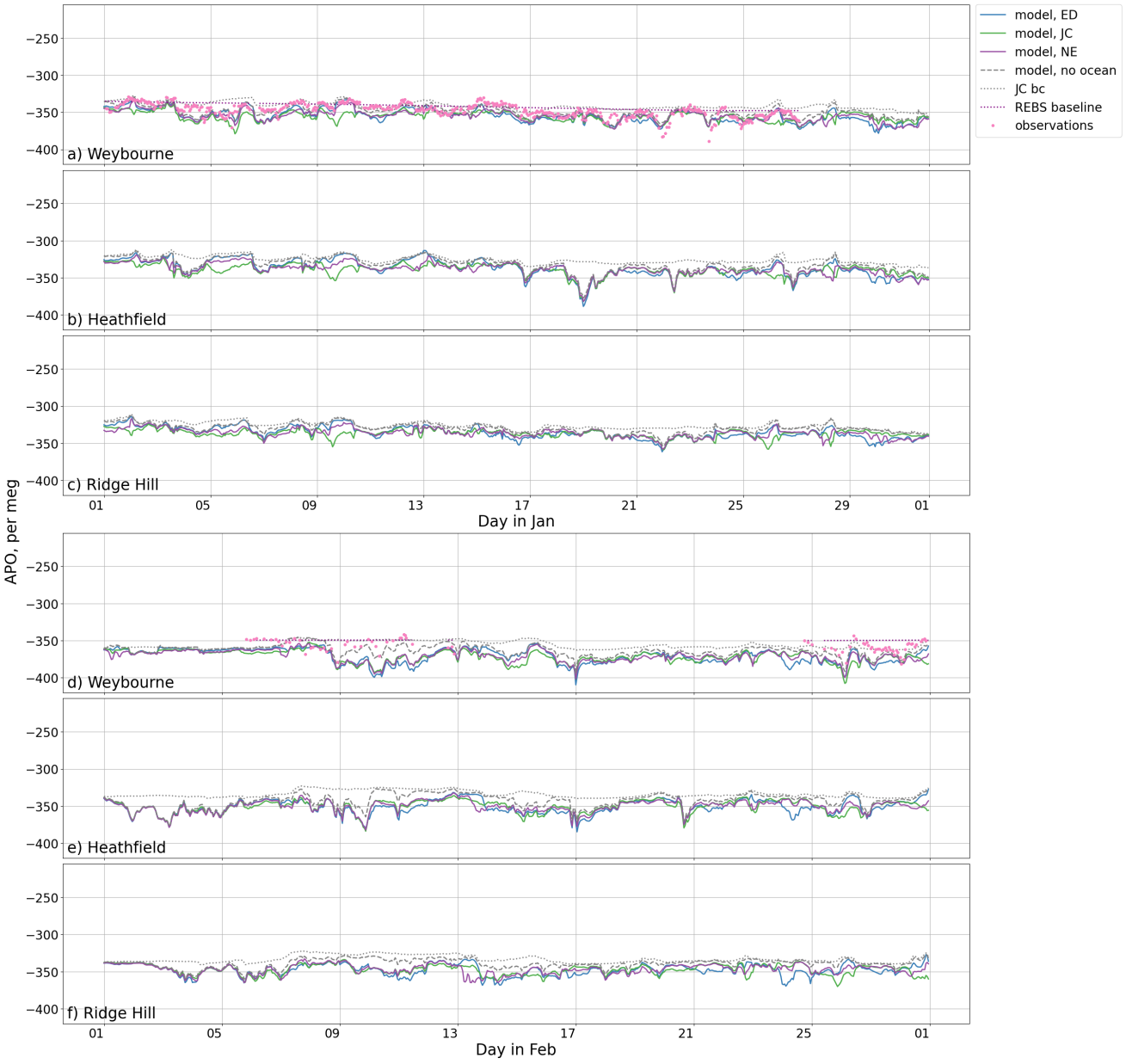

Figure 3. The modelled and observed APO at Weybourne, Heathfield, and Ridge Hill, where we model APO using three different ocean flux estimates from: the global ED ocean model (blue), the global JC inversion (green), and the regional NE ocean model (purple). We also show a model of APO excluding any ocean contribution (grey).

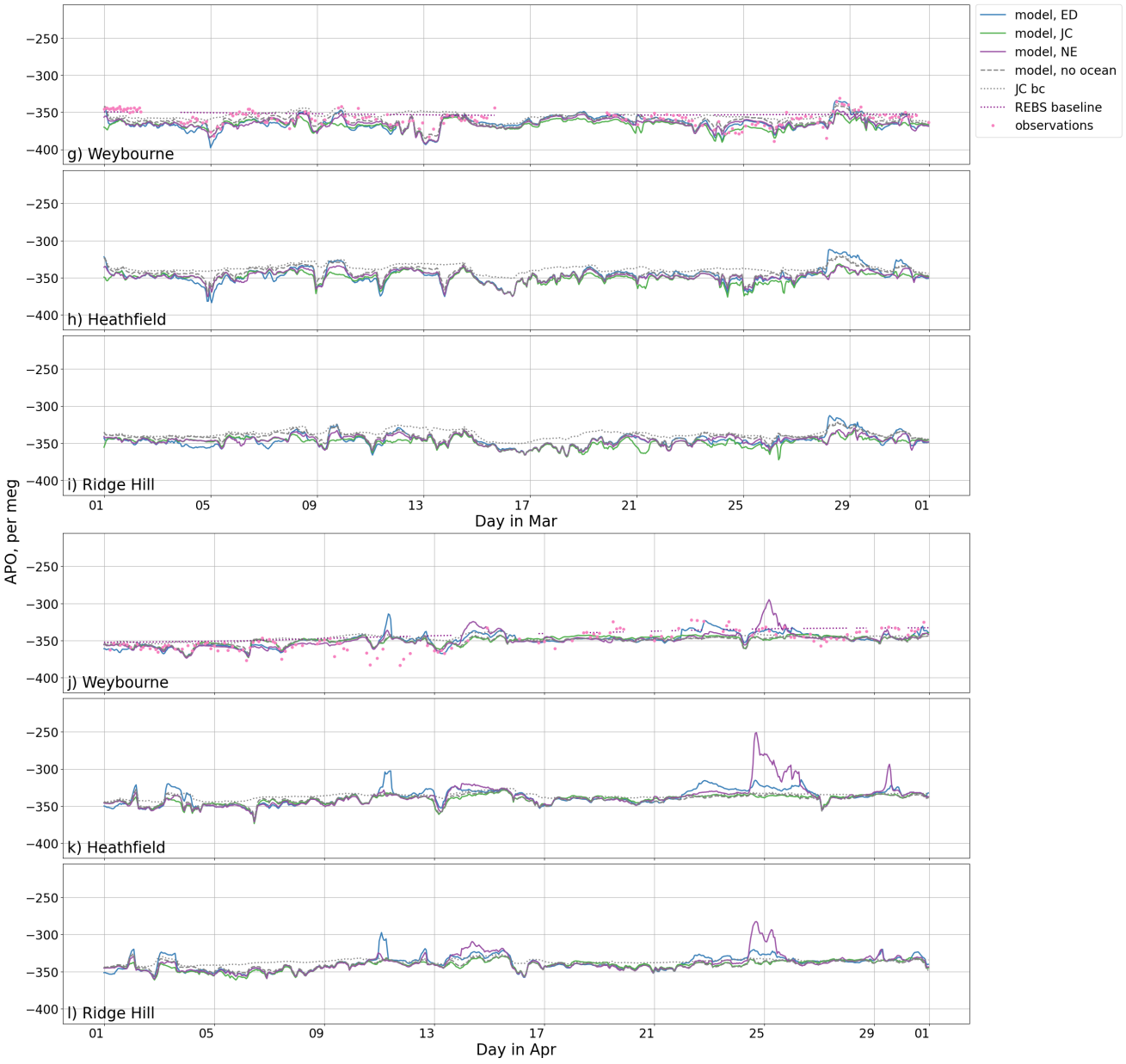

Figure 3. continued: the modelled and observed APO at Weybourne, Heathfield, and Ridge Hill, where we model APO using three different ocean flux estimates from: the global ED ocean model (blue), the global JC inversion (green), and the regional NE ocean model (purple). We also show a model of APO excluding any ocean contribution (grey).

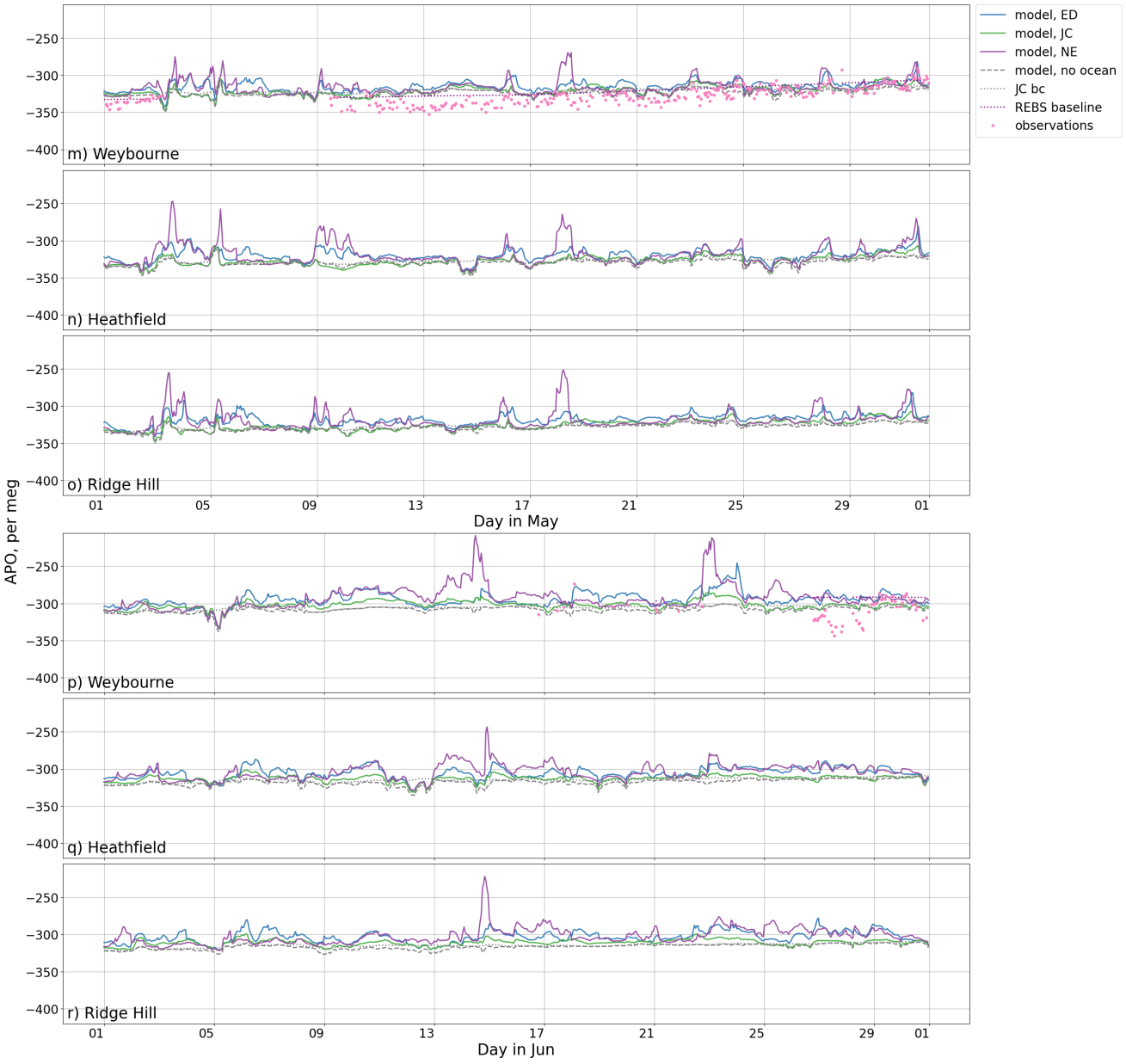

Figure 3. continued: the modelled and observed APO at Weybourne, Heathfield, and Ridge Hill, where we model APO using three different ocean flux estimates from: the global ED ocean model (blue), the global JC inversion (green), and the regional NE ocean model (purple). We also show a model of APO excluding any ocean contribution (grey).

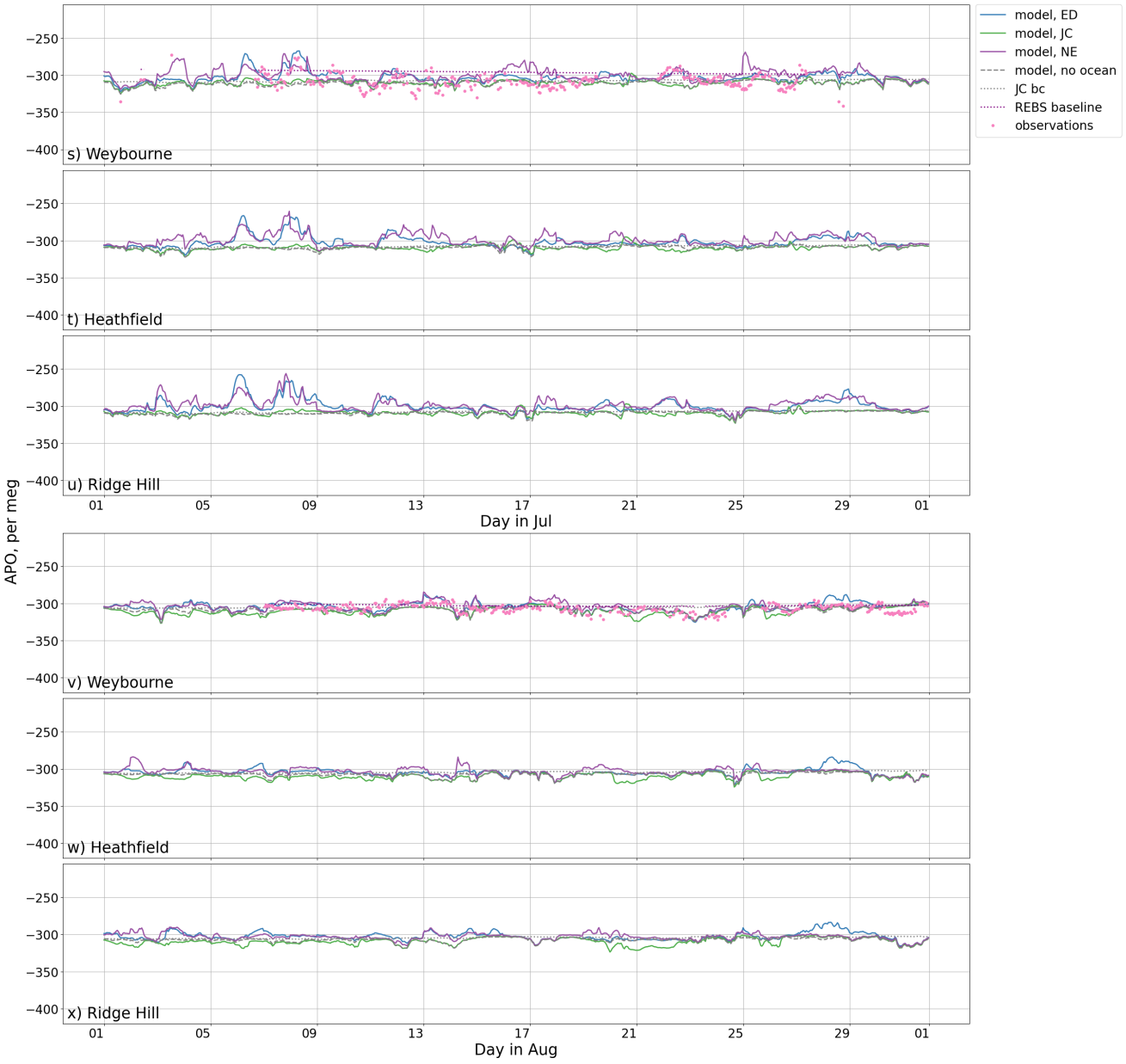

Figure 3. continued: the modelled and observed APO at Weybourne, Heathfield, and Ridge Hill, where we model APO using three different ocean flux estimates from: the global ED ocean model (blue), the global JC inversion (green), and the regional NE ocean model (purple). We also show a model of APO excluding any ocean contribution (grey).

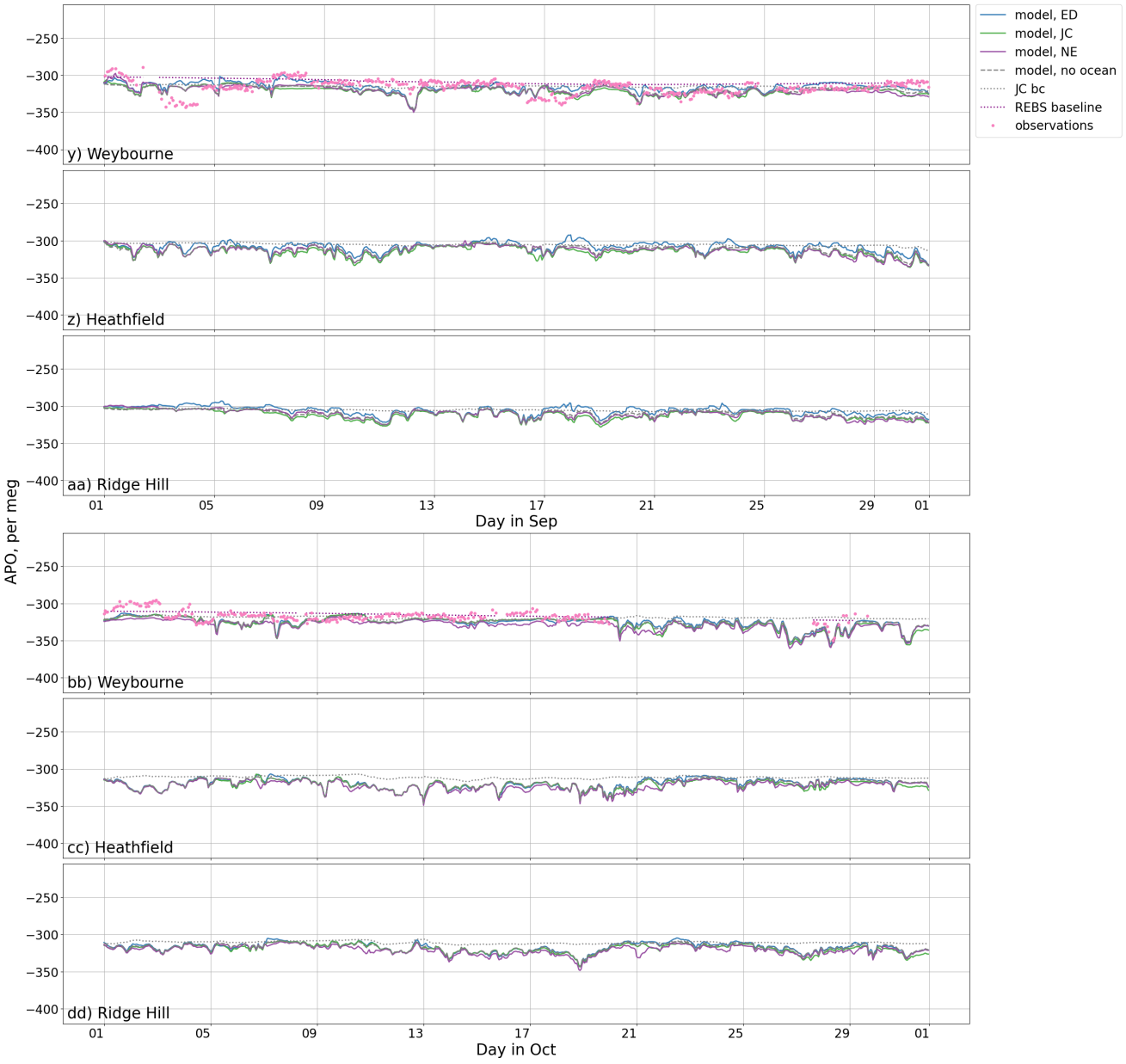

Figure 3. continued: the modelled and observed APO at Weybourne, Heathfield, and Ridge Hill, where we model APO using three different ocean flux estimates from: the global ED ocean model (blue), the global JC inversion (green), and the regional NE ocean model (purple). We also show a model of APO excluding any ocean contribution (grey).

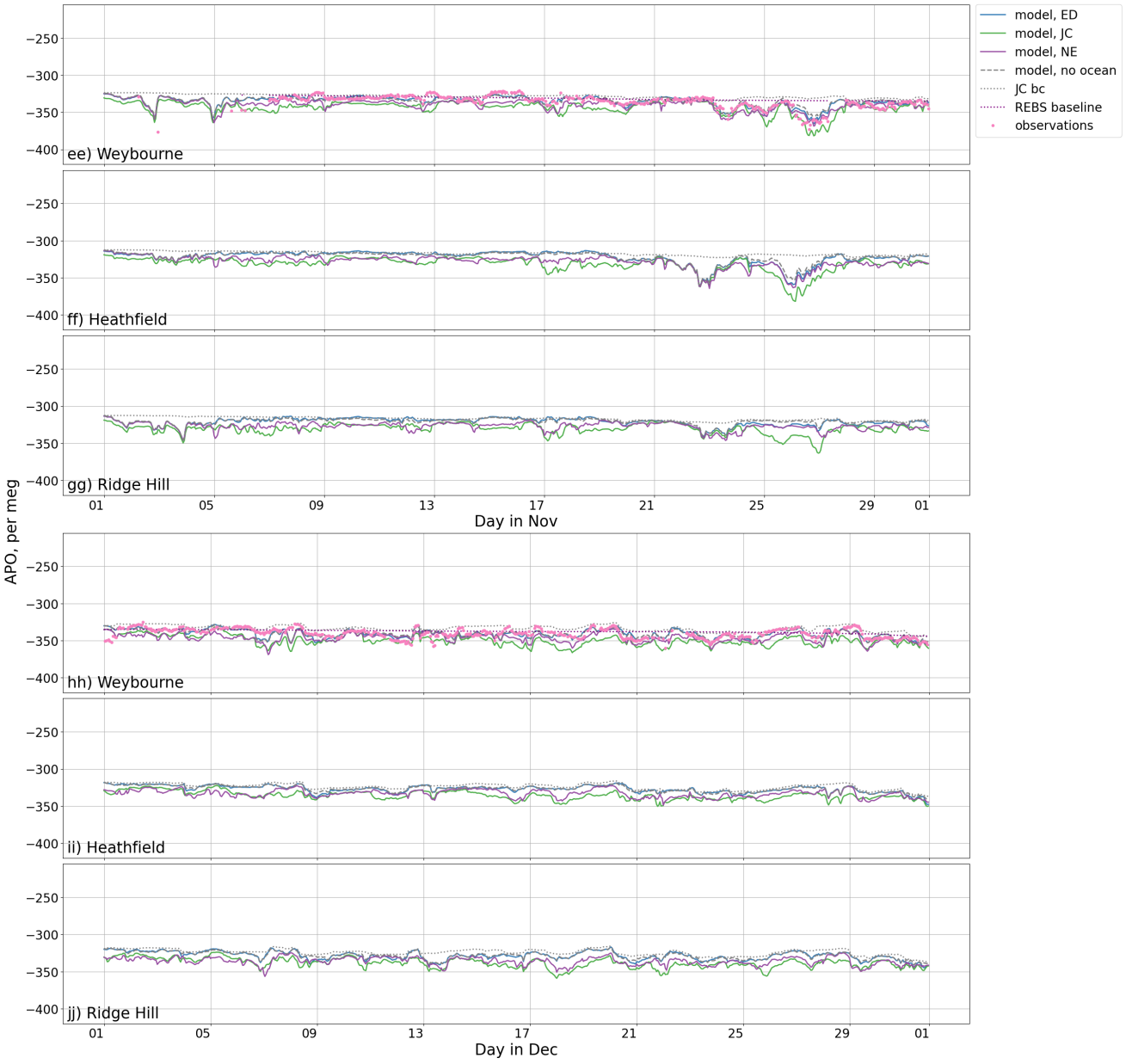

Figure 3. continued: the modelled and observed APO at Weybourne, Heathfield, and Ridge Hill, where we model APO using three different ocean flux estimates from: the global ED ocean model (blue), the global JC inversion (green), and the regional NE ocean model (purple). We also show a model of APO excluding any ocean contribution (grey).

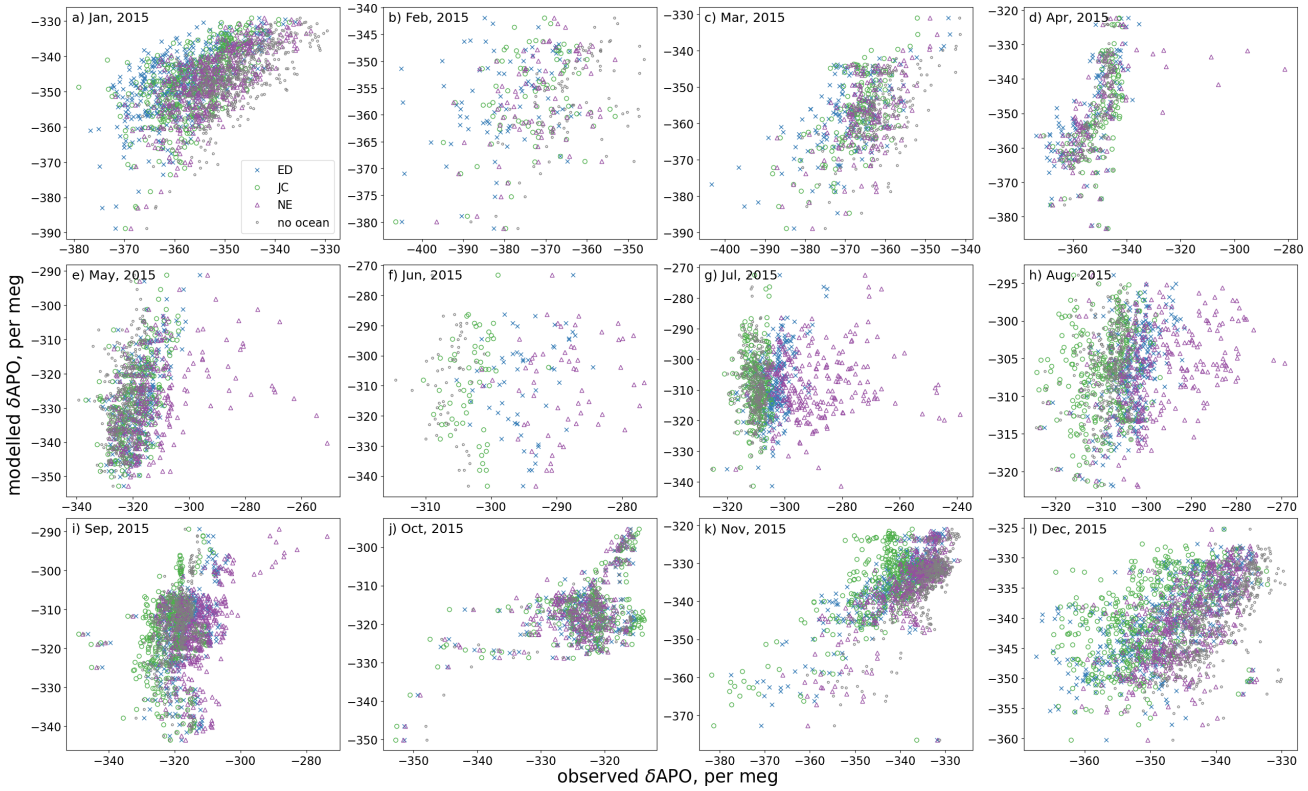

Figure 4. The modelled and observed APO at Weybourne throughout 2015 where we model APO using three different ocean flux estimates from: the global ED ocean model (blue crosses), the global JC inversion (green circles), and the regional NE ocean model (purple triangles). We also show a model of APO excluding any ocean contribution (small grey circles).

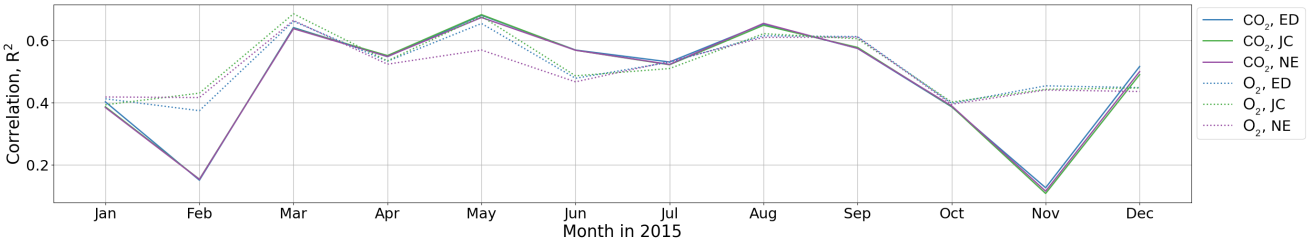

Figure 5. The Pearson correlation coefficient (R^2) for modelled and observed hourly CO_2 (solid lines) and O_2 (dotted lines) mole fractions at Weybourne for each month throughout 2015. The blue, green, and purple lines show the results from the models derived using the NAME simulations and either ED, JC, and NE ocean fluxes, respectively.

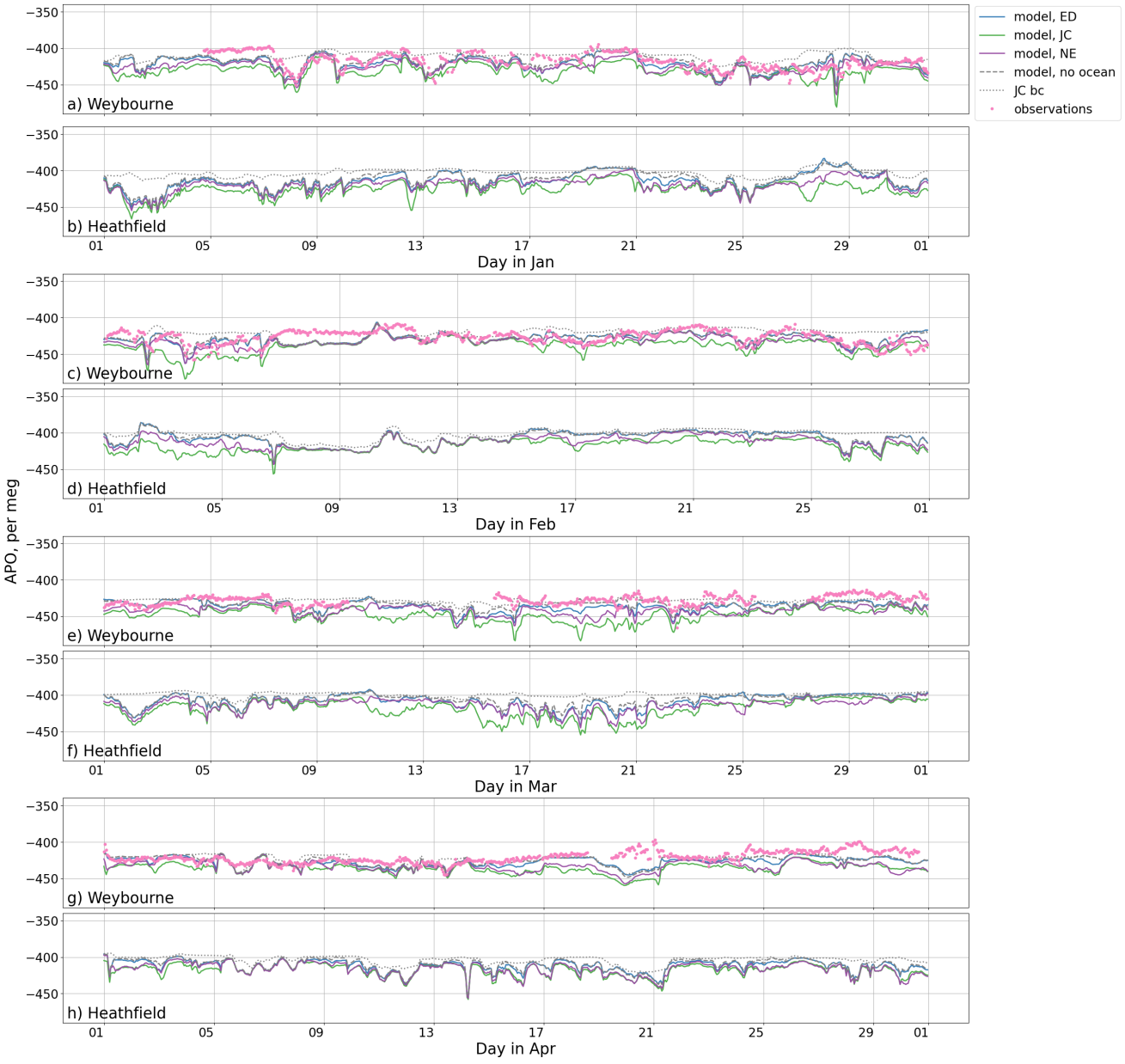

Figure 6. The modelled and observed APO abundance at Weybourne, Heathfield, and Ridge Hill in 2021. We model APO using three different ocean flux estimates from: the global ED ocean model, the global JC inversion, and the regional NE ocean model.

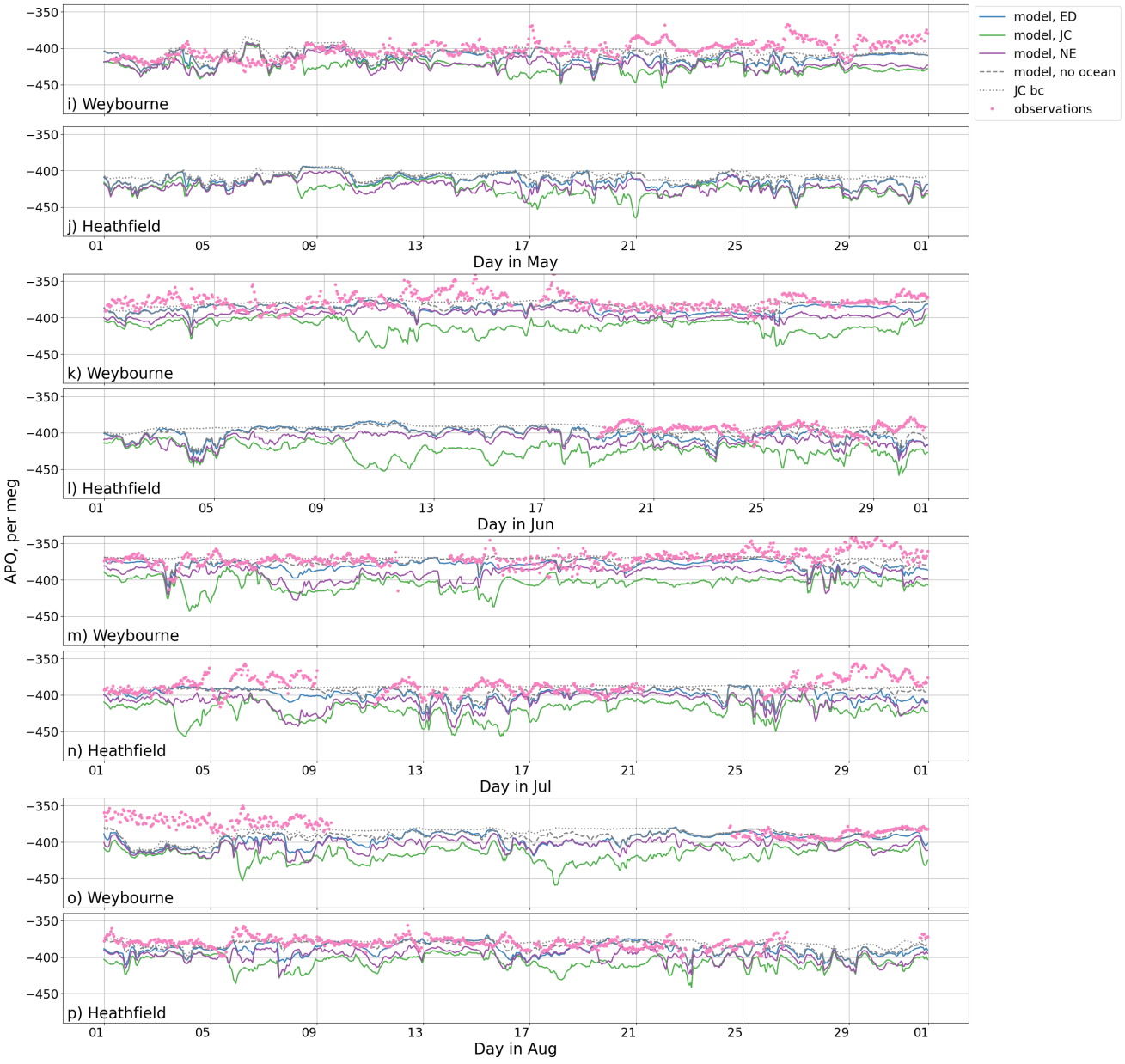

Figure 6. continued: the modelled and observed APO abundance at Weybourne, Heathfield, and Ridge Hill in 2021. We model APO using three different ocean flux estimates from: the global ED ocean model, the global JC inversion, and the regional NE ocean model.

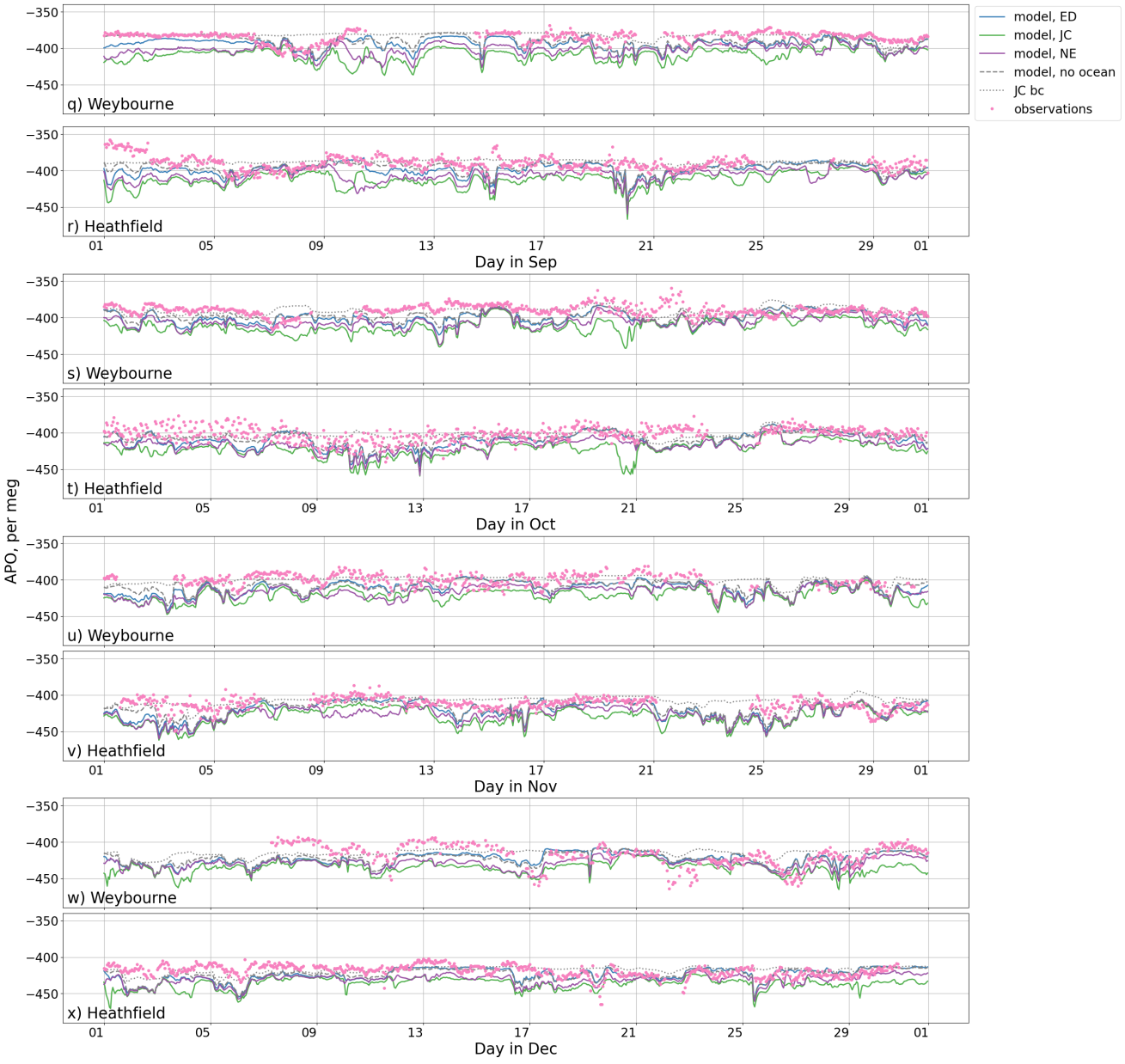

Figure 6. continued: the modelled and observed APO abundance at Weybourne, Heathfield, and Ridge Hill in 2021. We model APO using three different ocean flux estimates from: the global ED ocean model, the global JC inversion, and the regional NE ocean model.

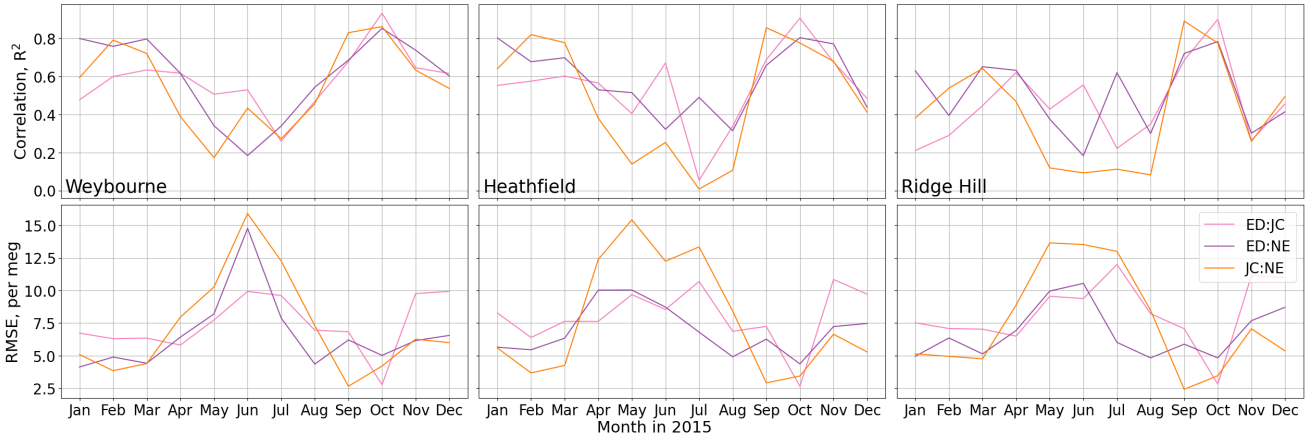

Figure 7. The comparison of APO NAME simulations using three different estimates for the ocean O_2 flux, where the top panel displays the Pearson correlation coefficient (R^2) between models, and the bottom panel displays the RMSE. The pink line shows the comparison between the models using the ED and JC estimates, the purple line shows that between the models using the ED and NE estimates, and the orange line shows that between the models using the NE and JC estimates.

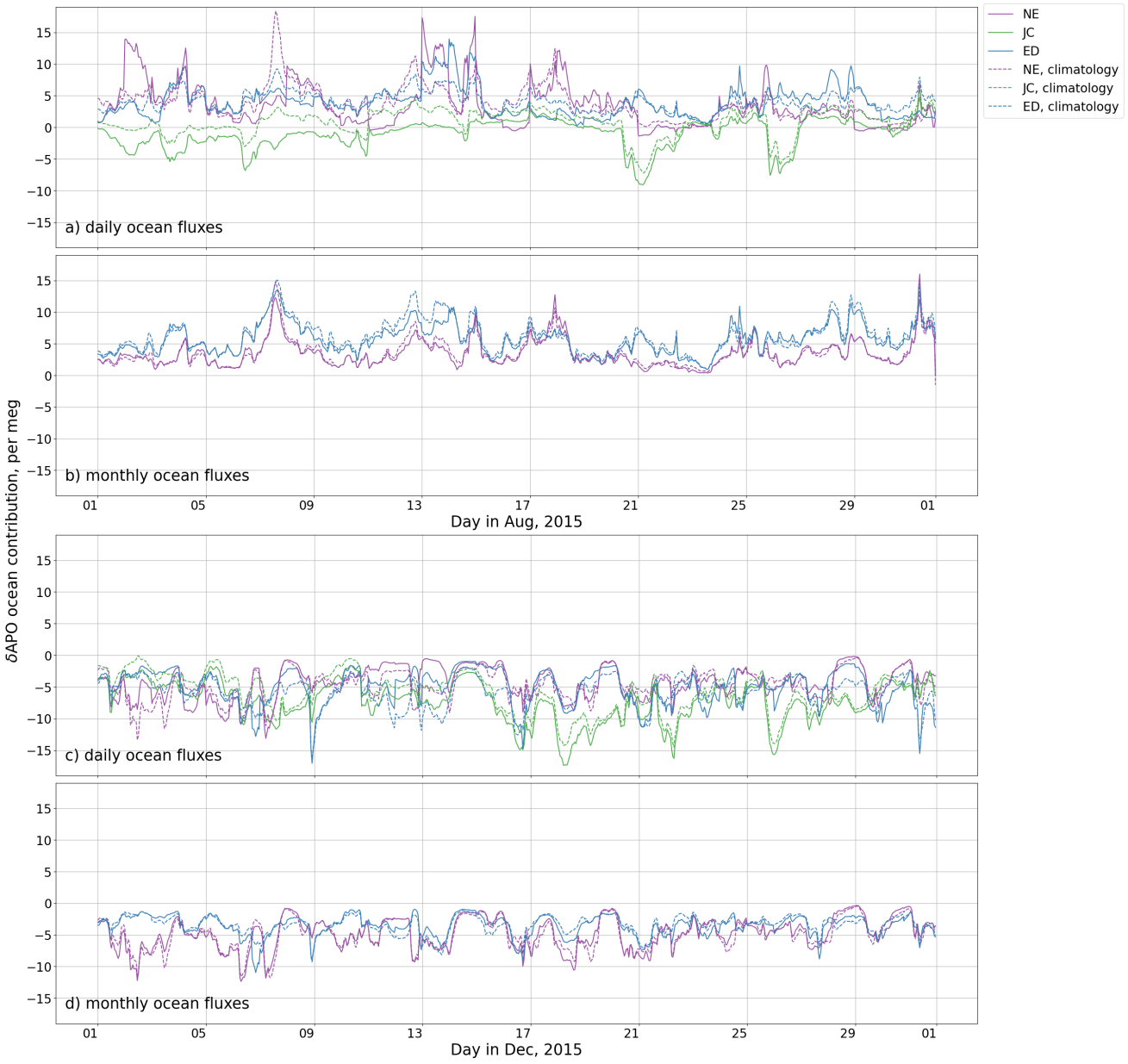

Figure 8. The regional oceanic contribution of APO to the abundance at Weybourne during August *(panels a and b)* and December *(panels c and d)* 2015, estimated by the ED and NE simulations and the JC inversion, also comparing the 2015 flux with an estimated climatology and the daily *(panels a and c)* and monthly *(panels b) and d)* O_2 time resolution.

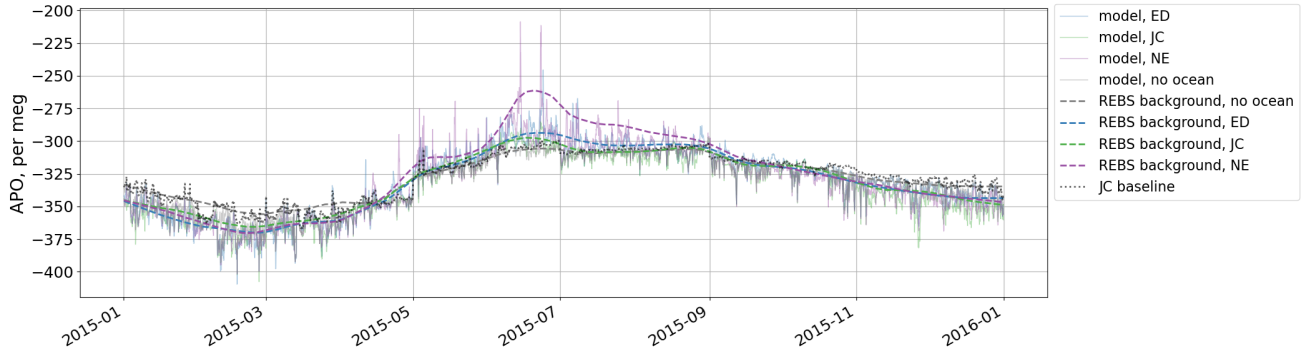

Figure 9. The APO models (solid lines) and baselines fit to each model using REBS (dashed lines) throughout 2015, where the ED model and baseline are in blue, JC in green, NE in purple, and no ocean in grey. The adjusted JC baseline is shown by the black dotted line.

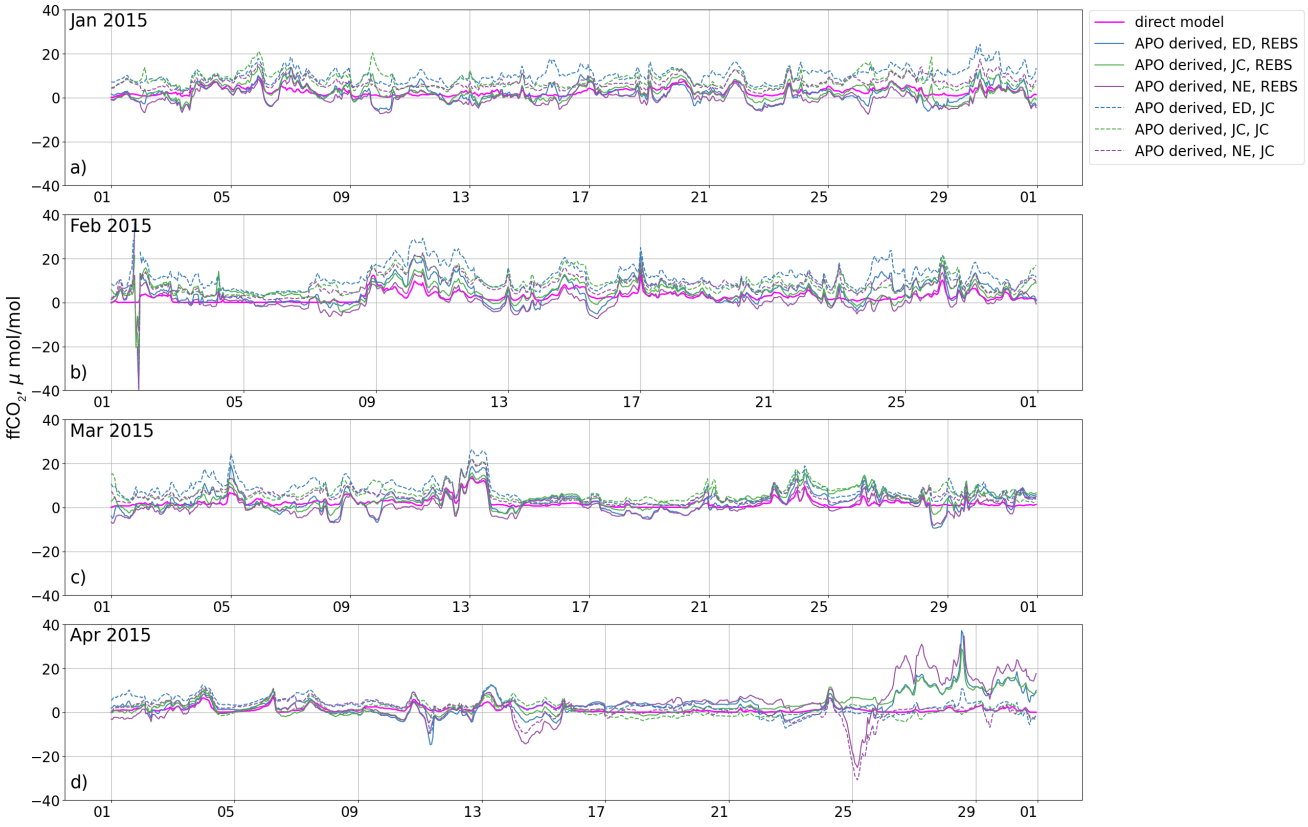

Figure 10. The modelled $ffCO_2$ derived from the APO model for Weybourne for January – April 2015. We compare the results from using three different ocean flux fields with the direct model estimated using the NAEI-within-EDGAR fluxes and NAME footprints, as well as two different method of background subtraction.

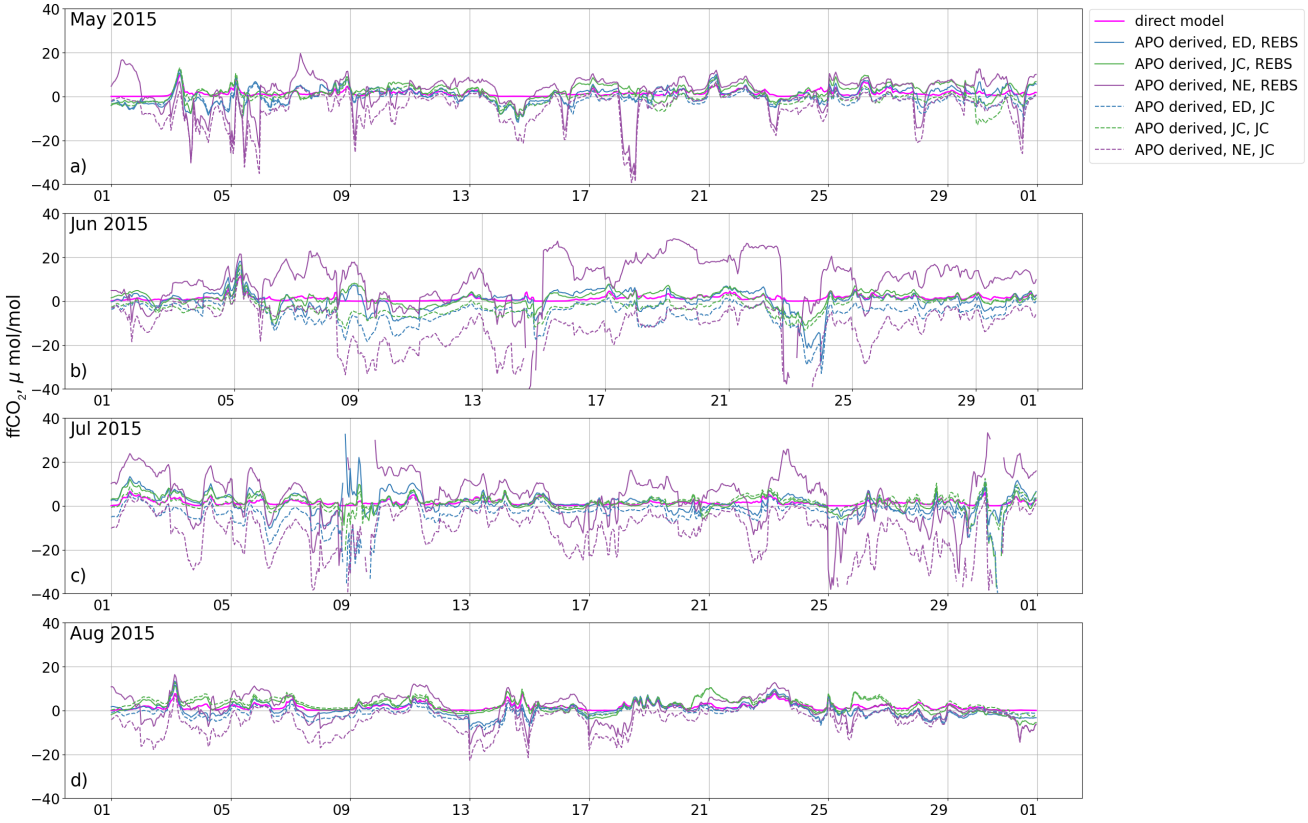

Figure 10. continued: The modelled $ffCO_2$ derived from the APO model for Weybourne for May – August 2015. We compare the results from using three different ocean flux fields with the direct model estimated using the NAEI-within-EDGAR fluxes and NAME footprints, as well as two different method of background subtraction.

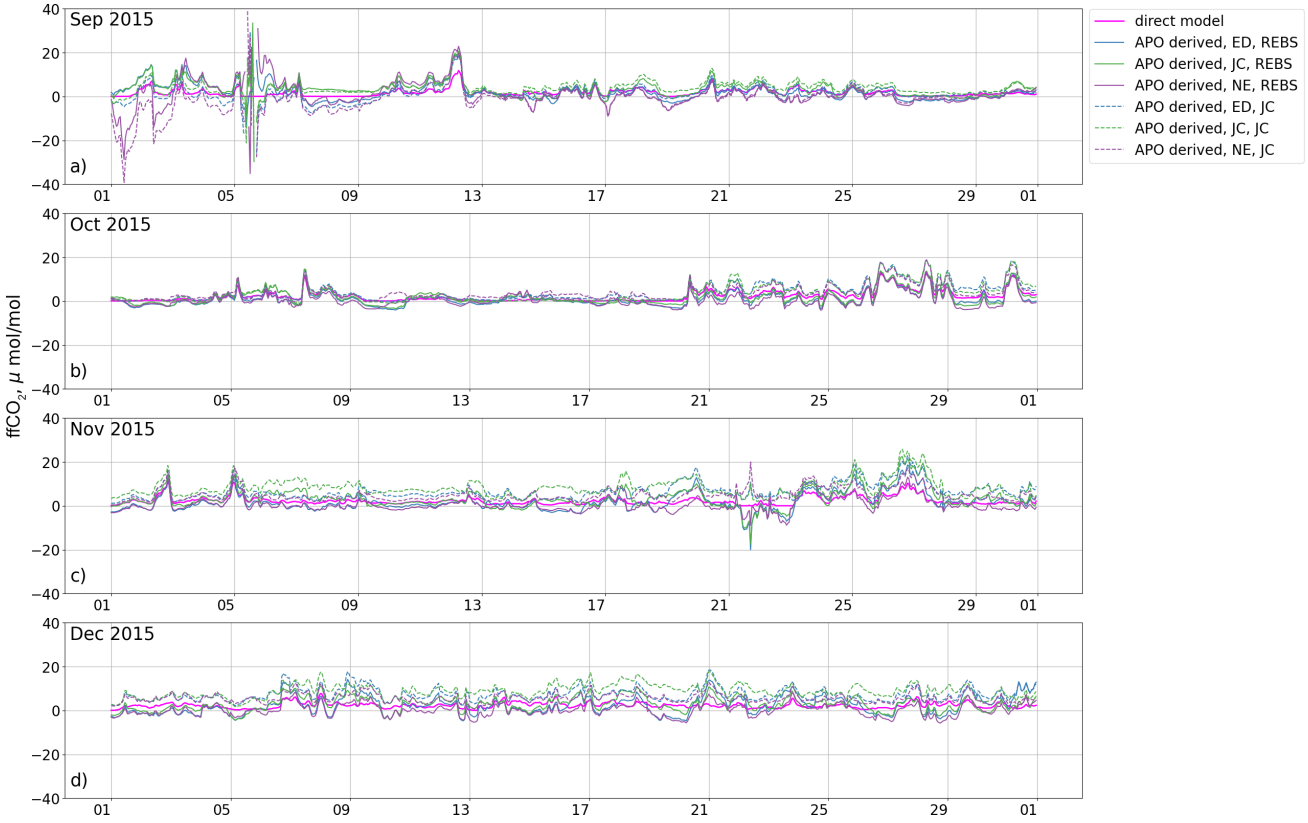

Figure 10. continued: The modelled $ffCO_2$ derived from the APO model for Weybourne for September – December 2015. We compare the results from using three different ocean flux fields with the direct model estimated using the NAEI-within-EDGAR fluxes and NAME footprints, as well as two different method of background subtraction.